Design, fabrication, and characterization of a facile superhydrophobic and superoleophilic mesh-based membrane for selective oil-water separation

Rasouli Seyedabbas, Rezaei Nima, Hamedi Hamideh, Zendehboudi Sohrab, Duan Xili

DOI: 10.1016/j.ces.2020.116354

Design, Fabrication, and Characterization of a Facile Superhydrophobic and Superoleophilic Mesh-Based Membrane for Selective Oil-Water Separation

Seyedabbas Rasouli[1], Nima Rezaei[1,2], Hamideh Hamedi[1], Sohrab Zendehboudi[1]*, Xili Duan[1]

[1]Faculty of Engineering and Applied Science, Memorial University, St. John's, NL, Canada

[2]Department of Separation Science, Lappeenranta-Lahti University of Technology, Finland

*Email address of the corresponding author: szendehboudi@mun.ca

ABSTRACT

Superhydrophobic and superoleophilic (SHSO) membranes have found great attention in oil-water separation application. We fabricate a SHSO stainless steel mesh-based membrane, using a facile one-stage dip-coating technique, and investigate the effects of silane alkyl chain, and ratio of micro-to-nanoparticles in the coating. Silane compounds with short- and long-alkyl functional chains (Dynasylan® Sivo 408 and Dynasylan® F8261, respectively) are used as surface energy modifiers. To create hierarchical morphology, Aerosil® R812 and SIPERNAT® D13 are employed as the nano and microparticles, respectively. The long-silane features a higher water contact angle (WCA) at all solid compositions. Increasing ratio of nano-to-microparticles increases the WCA with long-chain silane. Maximum WCAs=165.8˚and 164.2˚are attained with the long and short silanes, respectively, when the coating solid is composed of 75 wt% nanoparticles and 25 wt% microparticles. Increasing the concentration of nanoparticles to 100% decreases hydrophobicity, which is more pronounced for the short-chain silane. The WCA decreases to 163.8˚ and 155.5˚ for the coating solutions containing the long and short silanes, respectively, with 100% nanoparticles to modify the surface roughness. Flower-like hierarchical roughness structures are observed using the coating solution of silanes with only nanoparticles. The average pore opening for the mesh decreases from 76 μm in the bare mesh to 48 μm for the coated mesh. Analytical surface characterization results (e.g., sliding angle, energy-dispersive X-

ray spectroscopy (EDX), and Fourier transform infrared spectroscopy (FTIR)) confirm the SHSO features of the as-prepared mesh. Except for the exposure to 1.0 M NaOH solution, the membranes are stable (WCA>145˚) in H_2SO_4, NaOH, and NaCl solutions over four weeks. Using the fabricated mesh, the macroscopic separation efficiency of kerosene from water is > 99%. The membrane fabrication strategy proposed in this study further highlights the importance of the SHSO wetting condition in the effective treatment of oily wastewater streams in a variety of food, chemical, and energy industries.

Keywords: Superhydrophobic, Superoleophilic, Oil/water separation, Contact angle, Mesh

1 INTRODUCTION

Superhydrophobic and superoleophilic (SHSO) surfaces are commonly used in the form of porous or mesh material in oil-water separation applications such as the treatment of oily wastewater and oil spill removal. The mesh-based SHSO membranes feature a higher permeability and mechanical strength, and a lower pressure drop compared to the porous membranes. Among the metallic mesh substrates, stainless steel (SS) and copper materials are commonly used as the base substrate; its wettability is altered to SHSO condition by modifying surface morphology and chemistry. In the literature of SHSO SS mesh membranes, methods such as acid erosion [1-3], colloidal assembly [4-12], rough polymer film [13, 14], crystal growth [15-17], and chemical vapor deposition (CVD) [18-20] are used to create hierarchical micro- and nano roughness features. For the SS mesh membranes, chemicals such as fluoropolymers [17, 18, 21], silanes [1, 11], stearic acid [2, 5, 6, 9, 12, 15], and thiols [10] are commonly used to adjust the surface energy to achieve SHSO wetting.

In this section, we present a history of SHSO SS mesh membranes that are used in oil-water separation application. The first SHSO membrane was fabricated by Feng et al. [4] in 2004 through spray-coating a mixture of polytetrafluoroethylene (PTFE) particles, polyvinyl acetate (as an adhesive), polyvinyl alcohol (as a dispersant), water (as a thinner), and sodium dodecylbenzylsulfate (as a surfactant) on SS

mesh. The coating gel was cured at 350˚C to improve the coating stability; the coated mesh featured a water contact angle (WCA) of 156.2˚, an oil contact angle (OCA) of zero, and a sliding angle of 4˚ [4]. Since 2004, different facile approaches, including rough polymer films and colloidal assemblies, were employed to prepare SHSO membranes [7, 8, 10, 13, 14, 21-40]. For example, Yang et al. [13] coated a SS mesh with epoxy/attapulgite (44.4 wt%) through spray-coating, resulting in a WCA of 160˚± 1 and 98% oil-water separation efficiency. Xiang et al. [7] coated Ni, Fe, and Cu clusters onto a SS mesh, by grafting *n*-dodecyl mercaptan through polydopamine solution, and using electrodeposition process. They observed popcorn-like micro- and nano-roughness structures that were obtained by the particle clusters [7]. The as-prepared mesh exhibited a WCA of 162 ± 1°, with 98.6% oil-water separation efficiency. Cao et al. [9] spray-coated a mixture of phenol formaldehyde and $Mg(OH)_2$ nanoparticles (NPs) in stearic acid, onto a SS mesh. They found a WCA of 151.4˚, and oil-water separation efficiency of 94.6% (for soy oil) up to 10 separation cycles [9]. Matin et al. [8] spray-coated a suspension of CeO_2 NPs (with size distribution 100–500 nm) in tetrahydrofuran (THF) onto a SS mesh, following calcination at 200˚C (without further chemical modifications). The fabricated SHSO mesh with CeO_2 NPs agglomerated on the surface showed a WCA of 153˚ and an OCA of 0˚. Du et al. [2] used HF acid etching, following dip coating in a solution of stearic acid and Ag NPs. The SHSO SS mesh featured a WCA of 152˚ with an excellent stability against chemicals and hot water; they also observed over 97% oil-water separation efficiency (up to 40 cycles). In several studies, carbon nano tube (CNT) has been also used to fabricate the SHSO SS mesh [19, 41, 42]. Lee et al. [18] grew vertically aligned multi-wall CNTs on the SS surface via CVD in the presence of Al_2O_3 diffusion barrier. The fabricated SHSO mesh resulted in a maximum WCA of 152˚; the mesh also successfully separated oil-in-water emulsions with an oil droplet size 3–100 μm, and oil concentration of 5–10 wt.%. Fluorinated (co)polymers such as PTFE or Teflon AF® have high chemical, thermal, and mechanical stabilities (against abrasion) that are naturally hydrophobic and oleophilic. With adding hierarchical micro- and nano roughness structure, the condition

of SHSO can be achieved. Wu et al. [17] used hierarchical rod- and flower-like roughness features of ZnO (1–2 μm) onto SS mesh, and coated it with Teflon AF®. ZnO was first seeded onto a SS mesh, by spraying 0.2 M zinc acetate solution. Using hydrothermal method, the hierarchical features were grown. The SHSO mesh had a WCA of 157˚ and the mesh was used for oil-water separation [17]. Varshney et al. [3] employed a mixture of hydrochloric acid and nitric acid to create microstructure surface roughness, and then applied lauric acid to adjust the surface energy. The as prepared mesh was SHSO with a WCA of 171˚, and a sliding angle of 4˚; over 99% oil-water separation efficiency was achieved in their work [3].

Dip-coating into a colloidal solution combines the surface morphology and surface energy modification steps in one step when fabricating the SHSO membranes [43, 44]. This technique is simple, controllable, and reliable in which high-quality thin films with thickness 0.1–100 μm can be achieved [45]. Using mixtures of microparticles (MPs) and nanoparticles (NPs) in the coating solution increases surface roughness heterogeneity, and improves mechanical stability of the coated meshes [24, 46]. Despite extensive investigations on developing SHSO membranes for oil-water separation, the effect of size distribution of solids (MPs and NPs) in the colloidal coating solution has been overlooked in previous research studies. Zhang et al. [47] examined the effect of roughness by adding micro- and nanoparticles of $CaCO_3$ solids. They employed a two-step coating method where the surface roughness was first created and then treated with stearic acid. They used spin-coating to first deposit the rough features from a suspension of solids in poly(vinylpyrrolidone) onto a glass slide; after the film was dried, the glass slide was dipped into 20 mM stearic acid in *n*-hexane for a period of 10 days to change the surface energy. It was found that the optimum concentration of solids is 40 wt% and that the best superhydrophobicity is achieved using 2 wt% MPs and 38 wt% NPs (meaning that 95% of the solid is NP). Zhang et al. [47] concluded that among all compositions tested, only one solid composition satisfies the sliding angle<10° condition for the hydrophobic surfaces [47,48]. One issue with the experimental

methodology is that the centrifugation force is expected to cause heterogeneity in the size of solid aggregates deposited onto the glass slide; larger particles will be pushed away from the rotation center. A simple one-step coating procedure is employed in this study where the surface roughness features (MPs and NPs of silica) and surface modification chemicals (two different organoalkylsilanes with short- and long alkyl-chains) are simultaneously present in the coating solution. We use Dynasylan® F8261 as long silane, and Dynasylan® SIVO 408 as the short silane; there is no study in the literature on SHSO SS mesh membranes using the shorter silane. Organoalkylsilanes with a longer fluorinated alkyl chain are known to be more hydrophobic. However, fluorine (F) is harmful to the environment and it is desired to use less F in the coating solution. One practical implication from our research is that it is possible to use a shorter silane and to compensate for its lower hydrophobicity by controlling the surface morphology—through adjusting the ratio of micro- and nanoparticles in the coating solution. We also conduct systematic long-term stability of SHSO membranes in concentrated alkaline, acidic and brine solutions.

The structure of the paper is designed as follows. After the introduction part in Section 1, materials and methods for fabricating and characterizing the superhydrophobic and superoleophilic membranes are discussed in Section 2. Advantages and disadvantages of the proposed experimental approach are summarized in Section 3. The results and discussions are provided in Section 4 where the results of WCA, sliding angle, transmission electron microscopy (TEM), scanning electron microscope (SEM), X-ray diffraction (XRD), Fourier-transform infrared spectroscopy (FTIR), energy-dispersive X-ray spectroscopy (EDX), and separation efficiency analyses are presented. Finally, in Section 5, the key conclusion remarks are summarized.

2 MATERIALS AND METHODS

2.1 Materials

Stainless steel 316 meshes (woven, 34% open area and 75 µm opening, and 53.3 µm wire diameter) are purchased from McMaster-Carr. Sulfuric acid (H_2SO_4, 98 wt%) is purchased from Caledon Laboratory Ltd. Hydrochloric acid (HCl, 37 wt%), hydrogen peroxide (H_2O_2, 30 wt%), and acetone (99.5 wt%) are obtained from ACP Chemicals. Dynasylan® F8261 solution (long-chain alkyl silane), Dynasylan® SIVO 408 (short-chain alkyl silane), hydrophobic SiO_2 nanoparticles (NPs) of AEROSIL® R812 (7 nm), and microparticles (MPs) of SIPERNAT® D13 (10.5 µm) are provided from Evonik Industries AG. Acetone and ethanol (> 99.5 wt%) are utilized for cleaning. Kerosene is purchased locally, and is used in oil-water separation tests. All chemicals are used without any purification. Compressed air is used for pre-drying. Deionized water (DI, 18.2 MΩ.cm) is produced in the lab (RODI-C-12A, Aqua Solution®).

2.2 Fabricating SHSO mesh

The fabrication process includes four main stages of a) cleaning, b) activation, c) solution preparation, and d) coating, as shown in Figure 1.

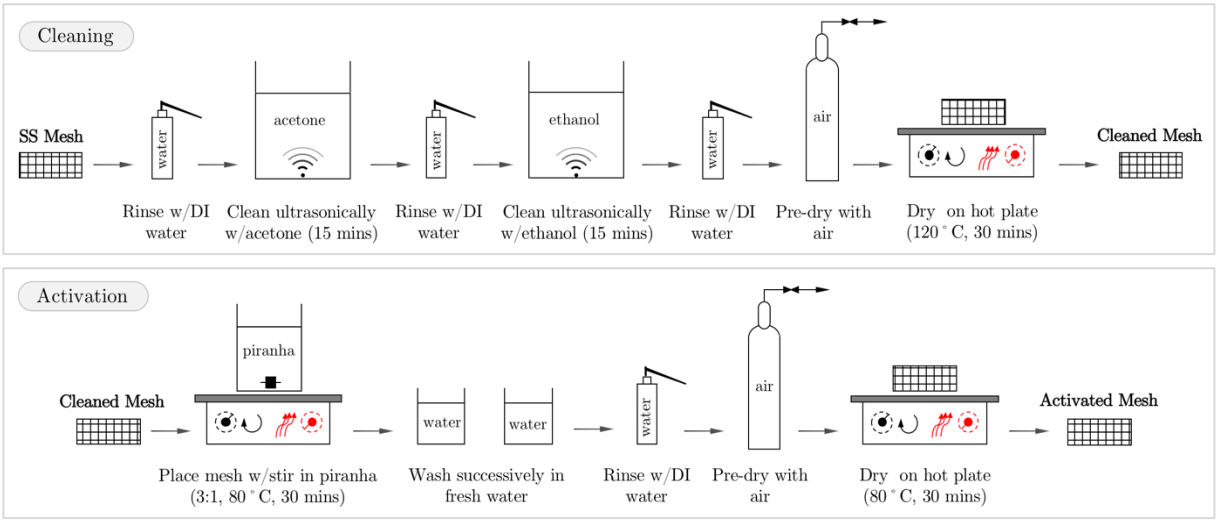

(a)

(b)

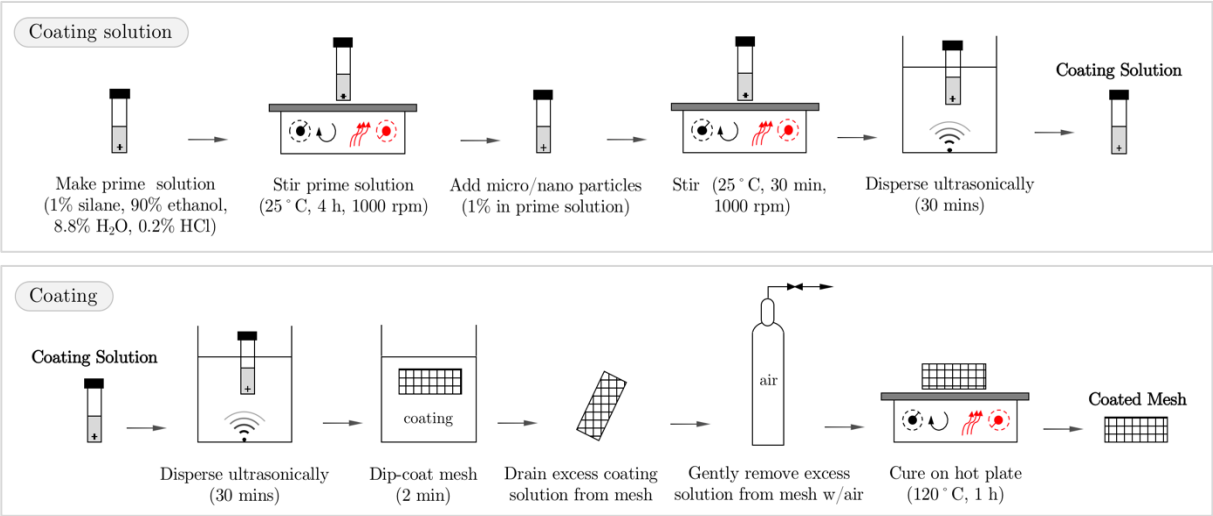

Figure 1. Schematics of the experimental procedures for (a) stainless steel mesh cleaning, (b) mesh activation, (c) coating solution preparation, and (d) mesh coating.

Cleaning: SS mesh samples (1 cm wide, 5 cm long) are cut and rinsed with DI water. The organic contaminants on the SS mesh surface are first ultrasonically cleaned (for 30 min) in acetone, rinsed with DI water, ultrasonically cleaned (for 30 min) in ethanol, and rinsed with DI water again, as shown in Figure 1(a). The mesh is pre-dried with compressed air and dried on hot plate at 120˚C for 30 min [49].

Activation: The old oxide layers on the SS mesh are replaced with fresh and reactive hydroxyl groups. We activate the cleaned mesh using piranha solution (see Figure 1(b)). A 3:1 (by volume) mixture of H_2SO_4 (98 wt%) and H_2O_2 (30 wt%) is prepared for activation. The cleaned meshes are placed in the piranha solution heated to 80˚C for 30 min, while continuously stirred the piranha solution under a hood. The piranha solution is extremely reactive and requires extreme safety cautions. After this stage, we remove the mesh from the solution, and submerge it in DI water. Then, the activated mesh is rinsed with the DI water, pre-dried with compressed air, and dried on a hot plate at 120˚C for 30 min. Some studies used a 1:1 mixture of acetone and ethanol for chemical cleaning [5].

Coating solutions: Different coating solutions are prepared as depicted in Figure 1(c). The prime solution contains ethanol, silane, H_2O, and HCl at concentrations 90, 1, 8.8, and 0.2 wt%, respectively. The prime solution is mixed at room condition, using a magnetic stirrer at 900–1200 rpm to obtain a homogeneous solution. In this study, we use two different types of silanes, namely Dynasylan® F8216 (long-chain), and SIVO 408 (short-chain). Other coating solutions are prepared, by adding 1% solid (MPs and NPs) to the prime solutions. For NPs and MPs, Aerosil ® R812 (hydrophobic, 7 nm diameter) and SIPERNAT® D13 (hydrophobic, D_{50} = 10.5 μm), respectively, are utilized. After adding solids, the coating solution is mixed in a vial placed on a magnetic hot plate at 1000 rpm for 30 min, and ultrasonically dispersed for 30 min. 12 coating formulations are obtained as summarized in Table 1. All coatings contain 1 wt% silane in the prime solution. For the samples containing solids, the overall solid concentration (NP, MP, or both) in the prime solution is 1 wt%.

Table 1. Coating formulations with different silanes and solid particles.

Coating Formulation	Silane Type (Dynasylan®)	Solid Composition (wt%)	
		Aerosil® R812 (7 nm)	SIPERNAT® D13 (10.5 μm)
F1 (Prime)	Dynasylan® SIVO 408 (short-silane)	0	0
F2		0	100
F3		25	75
F4		50	50
F5		75	25
F6		100	0
F7 (Prime)	Dynasylan® F8261 (long-silane)	0	0
F8		0	100
F9		25	75
F10		50	50
F11		75	25
F12		100	0

Mesh coating procedure: We use dip-coating method to fabricate the SHSO mesh (see Figure 1(d)). This SHSO coating technique has been employed by other researchers in oil-water separation applications [11, 15, 24, 45, 50-52]. The coating solution is ultrasonically dispersed for 30 min, and the mesh samples are dipped into the coating solution for 2 min. The excess coating solution is allowed to

drain under gravity. The coating solution is dried with air, and placed on the top of a heat plate to be cured at 120˚C for 1 h. The curing improves the coating stability [53].

The reaction mechanism between the hydroxyl groups on activated stainless steel mesh and silane is given in a series of reactions [54], namely, hydrolysis, condensation, adsorption, and covalent bonding (grafting), as given in Figure 2. First, the silane (Dynasylan® R8261) undergoes the hydrolysis reaction in the presence of an acid (HCl in our study) to produce silanol and three moles of ethanol. Then, three silanol molecules condense, and two moles of water is produced. The condensed silanol molecules adsorb onto the activated SS mesh surface; in this stage, hydrogen bonds form between the oxygen and hydrogen molecules on hydroxyl groups and those on the adsorbed silanol molecules. Finally, upon heating, covalent bonds are formed (grafted) between the silane and SS surface. The fluorinated functional group [$–(CF_2)_5–CF_3$] are exposed on the surface of SS mesh, providing it with a hydrophobic property.

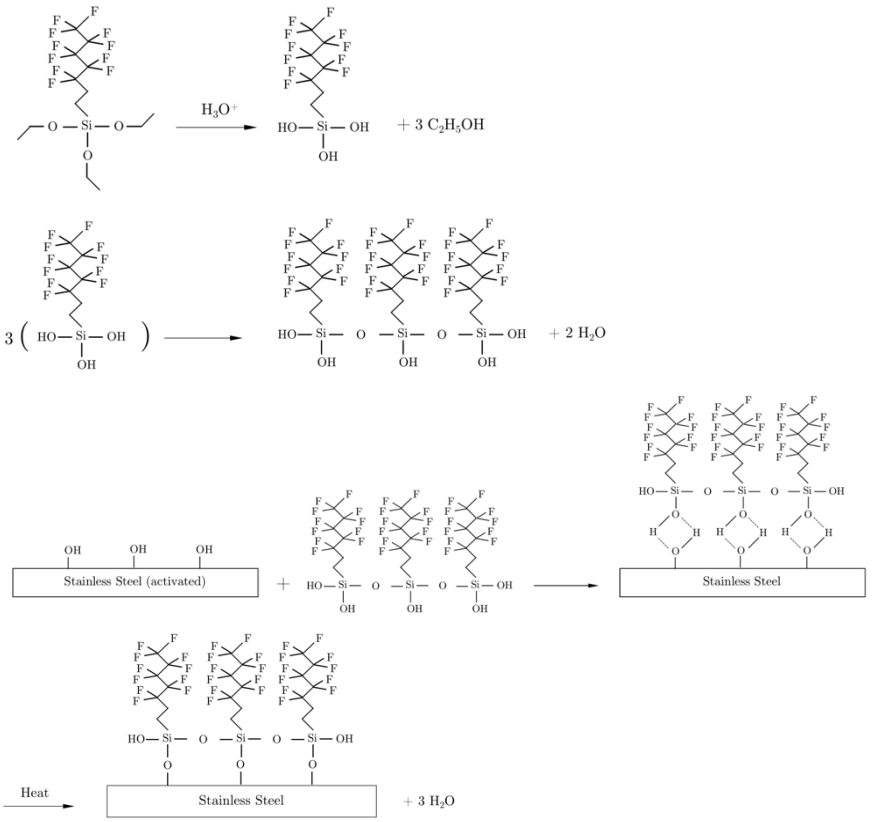

Figure 2. Mechanism of bonding between silane (Dynasylan® R8261) and activated stainless steel mesh (modified after Mostafaei et al. [53]). In this figure, different steps are given: (a) hydrolysis, (b) condensation, (c) adsorption through hydrogen bonding, and (d) covalent bonding (or, grafting).

2.3 Characterizing the SHSO mesh

We characterize the SHSO mesh, using static contact angle, sliding angle, stability analysis, transmission electron microscopy (TEM), scanning electron microscope (SEM), X-ray diffraction (XRD), Fourier-transform infrared spectroscopy (FTIR), energy-dispersive X-ray spectroscopy (EDX), and oil-water separation tests. Except for the static contact angle measurements, other characterization tests are conducted on the mesh samples coated with F12 (see Table 1). All experiments are conducted at ambient conditions. We measure WCA and OCA on dry mesh in the presence of air (OCA 15EC, DataPhysics Instruments GmbH, Germany). First, two pictures are taken from the top and front views to assure that the mesh is held straight and that the mesh openings are not stretched in any directions. Water droplets

of 10 μL are dispensed, using a Hamilton® syringe with a 20-gauge needle. For each mesh sample, we dispense three drops on different parts of the mesh, and report the average contact angle for each mesh. Also, for each drop, the right and left contact angles are measured and the average value is reported. For the sliding angle tests, the mesh holder assembly is tilted until the droplet starts to roll-off; receiving and advancing contact angles at the sliding state are measured at 34 fps.

For the stability tests, the SHSO mesh samples (coated with F12 formulation) are aged in 0.1 M and 1 M H_2SO_4, NaOH, and NaCl solutions for a period of up to four weeks. For each week, there are five replicated mesh samples in a sealed bottle, containing a chemical. The tests for 1 M chemicals are analyzed for one week.

The morphology and elemental analysis are characterized using FEI MLA 650FEG SEM equipped with Bruker EDX. In the SEM and EDX tests, we gold-sputter the coated mesh samples, and use a double-side carbon tape to attach them to an aluminum stub. The XRD patterns for the cleaned, silanized, and coated mesh samples (with F12) are conducted, using Rigaku Ultima-IV (40 kV and 44 mA). The scan starting angle and angle step are 30˚ and 0.02˚, respectively. The FTIR test is performed, using a Tensor II spectrometer (Bruker Instruments, Karlsruhe, Germany). We scratch the cured coating gel F12 of the mesh samples, and use it for the FTIR analysis.

The oil-water separation test is conducted according to Figure 3. A 1.27 cm ID ($^1/_2$ inch) mesh tube is functionalized with F12 coating solution, and is employed to separate free-oil from an oil-water mixture under gravity. The mesh is supported on a Swagelok® reducer fitting and is sealed with Teflon® shrink tube and a clamp. A 0.635 cm OD (¼ inch) tube is attached to the reducer fitting, and is passed through a rubber stopper that seals the bottom of a 2.54 cm (1 inch) glass tube. A valve is connected to the bottom of the separator. The hollow space between the tube mesh and the glass tube is filled with known amounts of kerosene and water with the valve closed. Then by opening the valve, oil is drained in the

coated mesh tube. By comparing the weights of the initial oil and collected oil, the separation efficiency is determined.

(a) (b)

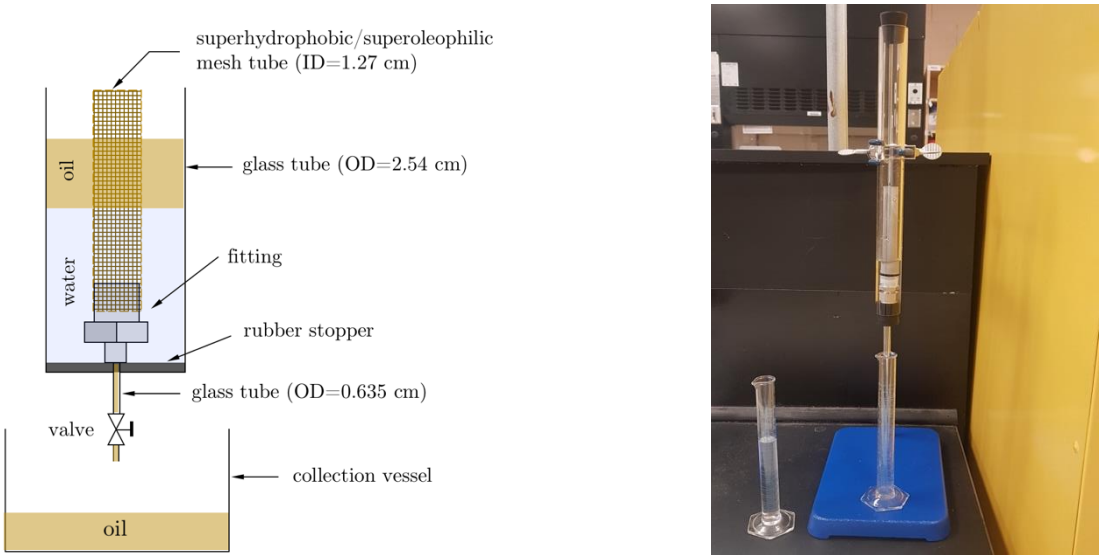

Figure 3. Oil-water separation experimental set up using SHSO mesh tube: (a) schematic picture, and (b) actual set up. Oil is shown in brown and water is shown in light blue color.

3 ADVANTAGES AND LIMITATIONS

This section further highlights the advantages of this experimental study as follows:

- This study introduces a fast and straightforward membrane fabrication method where the mesh surface chemistry and morphology are modified simultaneously.
- The SHSO coated mesh features a high stability in harsh conditions including strong alkaline and acid solutions, and highly aqueous saline solution; this highlights the quality of the coating obtained using an inexpensive one-step technique.
- Static oil-water separation using, a tubular mesh leads to more contact area/interface for the oil phase permeation through the SHSO surface. The excellent separation performance of the SHSO mesh obtained in the current study can be scaled up for large scale applications.

There are some drawbacks with our SHSO membranes as listed below:

- The silane coatings used for the surface modification might cause environmental concerns during membrane development and disposal.
- The roll welding of the stainless steel mesh may create weak points in terms of homogeneity of pore sizes that block water phase. This limits high operating pressures and flow rates as the larger pores (or fractures created during roll welding) cease water breakthrough.
- The SHSO coated mesh, with ~75 micron (nominal size) pore opening is not efficient for separating emulsified oil from an oil-water mixture where the oil droplets are smaller than the pore opening.

4 RESULTS AND DISCUSSIONS

This section reports wettability and stability assessments through contact angle measurements, surface characterization using TEM, SEM, XRD, FTIR, and EDX as well as oil-water separation efficiency.

4.1 Mesh wettability analysis

The activated SS mesh samples are coated with 12 different coatings F1–F12 (see Table 1). In all cases, the same SS mesh material is used. The oil (hexane) perfectly wets the mesh, giving a contact angle of zero. The effects of silane chain-length and solid (NPs and MPs) composition are investigated. The results of static WCA in the presence of air are demonstrated in Figure 4, as an average WCA for three drops repeated on three different mesh samples (a total of nine drops). The x-axis of Figure 4 shows the solid composition in the coating solution. The WCA results for the prime coatings F1 and F7 (0% NPs and 0% MPs) are also highlighted in Figure 4. The blue bars and gray bars represent the WCA results for the long-chain silane (Dynasylan® F8261) and the short-chain silane (Dynasylan® SIVO 408), respectively. WCA=124.3˚±2.8˚and 134.2˚±1.8˚ for the coatings with short silane (F1) and long silane (F7), respectively, are found. This observation is in agreement with findings in the literature that

hydrophobicity increases with the length of the silane functional chain [55, 56]. According to Figure 4, with increasing the fraction of the NPs in the coating within the range 0–75 wt%, the WCA increases. At the same level of wt%, the surface covered by the NPs (m^2 rough area/m^2 smooth area) is expected to be higher in the case of NPs. The hierarchical roughness pores can trap air to promote the condition for superhydrophobicity [24]. The increase in the WCA with the percentage of NPs (in the solid part) is more pronounced in the case of long-chain silane. For the short silane, the difference in the WCA within the range of NPs 0–50 wt% is statistically insignificant. There is a maximum WCA at the solid composition of 75% NPs and 25% MPs (see Figure 4). In all coatings that include solid, there is 1 wt% solid in the prime solution. At 75% NPs and 25% MPs solid composition, the WCA on the coating containing the short silane (F5) is 164.2˚±2.2˚ and that on the long silane (F11) is 165.8˚±2.0˚. By conducting a statistical *t*-test, it appears that the difference between the maximum contact angle achieved in long- and short-chain silanes (at 75% NPs and 25% MPs) is not statistically significant at 95% confidence level.

By increasing the NPs contribution in the solid to 100%, the contact angle on the coating with short silane (F6) decreases considerably, to 155.5˚±2.2˚, and that for the long silane (F12) decreases slightly, to 163.8˚±1.8˚. Therefore, among the solid concentration levels tested, the case containing 75% NPs and 25% MPs provides the highest hydrophobicity. Similarly, we conduct a t-test analysis at 95% confidence level on differences between the means of the two populations (for both silanes), to assess whether the optimality in the WCA on the coating with 75% NPs and 25% MPs is statistically different from that with 100% NPs only. Although the WCA difference is statistically significant (at 95% confidence) for the case of short-chain silane, it is not significant for the case of the long-chain silane. One problem in using a mixture of MPs and NPs in the dip-coating method is the likelihood of gravity settling for the larger particles. This may bring the concern with the coating homogeneity in terms of the solid particles on the mesh surface. Therefore, we use the coating solution F12 (with only NPs) for the remaining of

analysis to achieve a more homogeneous coating [57]; the long-chain silane also provides a slightly better hydrophobicity for which the difference between the WCAs on the coatings F11 (75% NPs) and F12 (100% NPs) is not statistically significant.

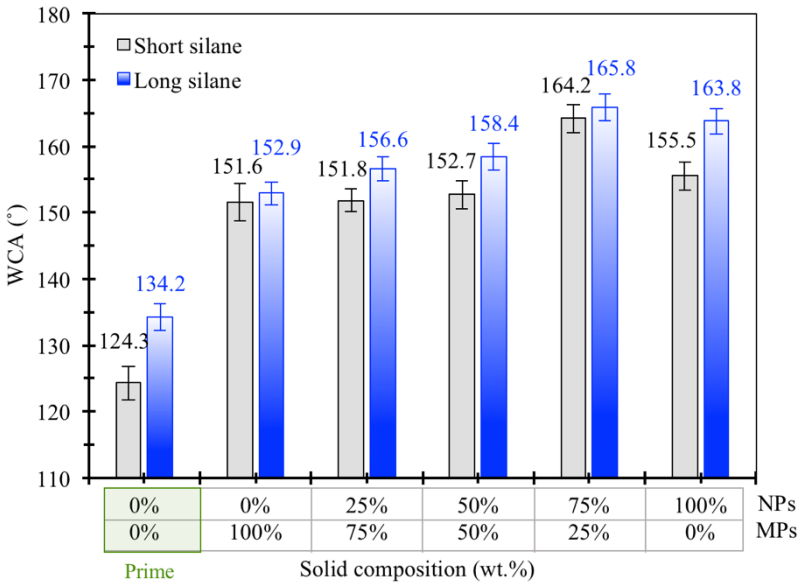

Figure 4. Static WCA on coated stainless steel mesh in the presence of air at ambient condition. The wt% of the NPs and MPs in the solid are given on the *x*-axis. The contact angle results are averaged for three replicates.

The results for the sliding angle measurements are shown in Figure 5. Right before water droplet sliding (see Figure 5(a)), the advancing and receding contact angles are measured at 155.9°±3.3° and 148.1°±3.0°, respectively. Therefore, contact angle hysteresis at the sliding condition is 7.7°±0.8° which satisfies the condition <10° for the hydrophobic surfaces [48].

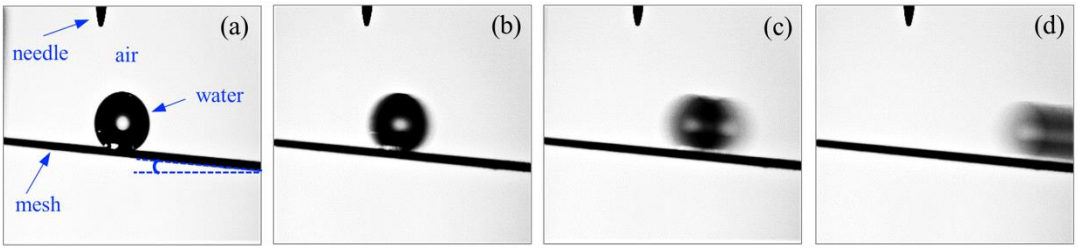

Figure 5. Snapshot of the water droplet starting to slide on an SHSO mesh (coated with F12) by increasing the inclination angle. The sliding starts in the frame (b).

4.2 Surface characterization analysis

Transmission electron microscopy (TEM): In this subsection, we present the TEM results from the NPs, MPs, and a 3:1 mixture of NPs to MPs (corresponding to 75 wt% NPs and 25 wt% MPs) as shown in Figure 6. A 5 wt% solution of solids in ethanol is prepared, following by 10 mins sonication for sample preparation. The TEM pictures are taken using Secnai™ Spirit TEM (FEI Company), using field emission electron of 80 kV, equipped with 4 Mega pixel AMG digital camera. The pictures demonstrate the morphology of the aggregates in Figure 6 for (a) NPs (alone), (b) MPs (alone), and (c) a 3:1 mixture of NPs and MPs (corresponding to 75% NPs in the solid compartment).

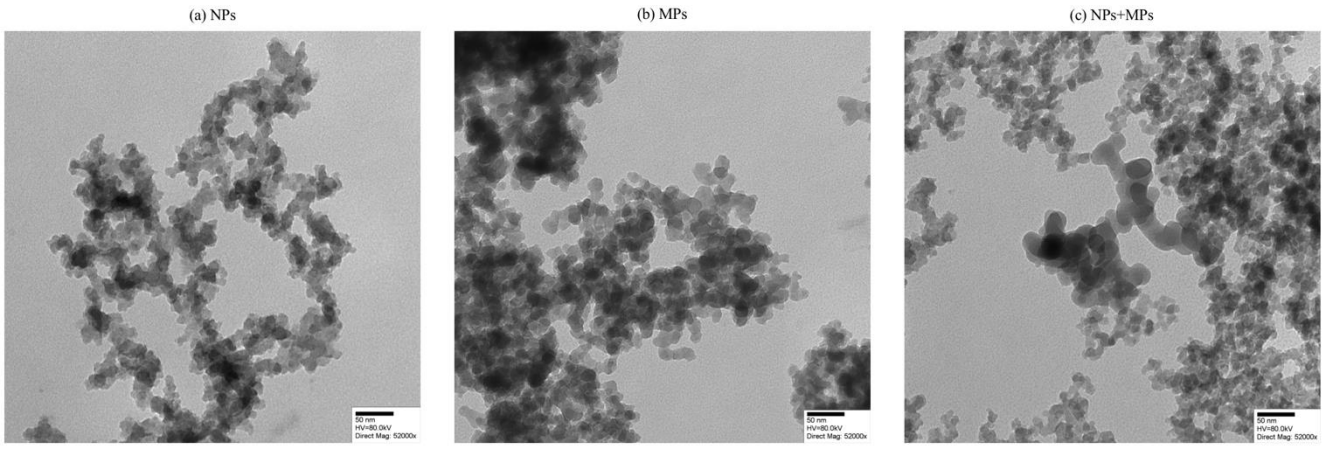

Figure 6. Transmission electron microscopy (TEM) pictures from solids used in the coating solution: (a) NPs (Aerosil® R812), (b) MPs (SIPERNAT® D13), and (c) mixture of NPs+MPs.

Scanning electron microscopy (SEM): We use SEM to visualize the morphology of the SHSO mesh membranes, coated with long-chain silane and a mixture of NPs and MPs. In Figure 7, the SEM pictures are shown for four characteristic coating solutions at 1,000X magnification; the bar scale is 100 (μm). The SEM picture in Figure 7(a) is for the SHSO mesh coated with the prime solution F7 (without any solids for roughness). Figure 7(b) depicts the SEM picture for the mesh with coating solution F8, containing 100% MPs in the solid part. Figure 7(c) includes the SEM picture for the coating solution F11 where the solid mixture contains 75% NPs and 25% MPs. As observed in Figure 4, the coating shown in Figure 7(c) gives the maximum WCA. The SEM picture for the mesh coated with solution F12, containing 100% NPs, is given in Figure 7(d). Among the four coating characteristic solutions, the coating solution F12 with 100% NPs provides flower-like hierarchical surface roughness with an extended surface area (see Figure 7). Referring to Figure 7(d), the fractures, which are observed within this flower-like surface roughness, have occurred during the drying and curing processes. The fractures provide regions of high capillary pressure for the oil (as the wetting phase), which are suitable for capturing smaller oil droplets from water when they are brought in contact with these high capillary regions. However, such a hierarchical surface roughness may cause membrane vulnerability to the fluids shear and impact by the solid contaminations in the liquid. As clear from Figure 7(b), the coating solution F8 with only MPs in the solid mixture does not uniformly cover the entire surface of the mesh material as some parts of the mesh are not covered with the rough solids. Because the MPs are heavier than the NPs, their faster sedimentation from the suspension solution might be the main reason for the lack of enough roughness on the mesh surface over a two-minute dip-coating. However, with additional surface roughness caused by the MPs, the WCA is increased from 134.2˚±1.8˚ (F7) to 152.9˚±1.8˚ (F8); the difference is statistically significant at a 95% confidence level. This increased contact angle with the added roughness is expected [51]. Moreover, Figure 7(c) reveals that the coating solution F11 with 75%

NPs and 25% MPs provides more roughness on the surface, compared to Figure 7(b). According to Figure 4, a statistically significant increase in the WCA values are observed because of the hierarchical roughness induced by the mixture of MPs and NPs in the coating. The WCA for the mesh shown in Figure 7(b) increases from 152.9˚±1.8˚ to 165.8˚±2.0˚ for the mesh corresponding to Figure 7(c).

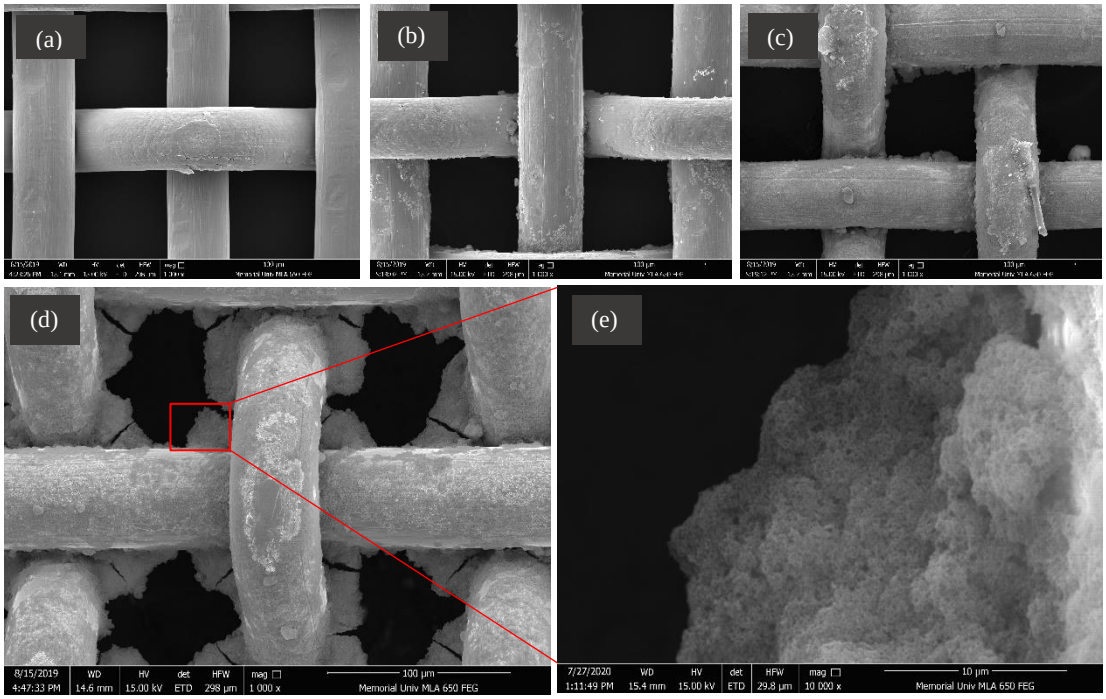

Figure 7. Scan electron microscopy of four SHSO mesh samples at 1,000X magnification: (a) silanized (F7), (b) F8 coating with 100% MPs, (c) F11 coating with 75% NPs and 25% MPs, and (d) F12 coating with 100% NPs, and (e) with magnification of 10,000X. The long-chain silane is used in all coatings. The nominal size of the mesh opening is 75 μm.

Comparing Figure 7(c) and 5(d), the flower-like roughness features are only observed for the coating, containing only NPs as solids (see Figure 7(d)). A better mechanical stability (against shear and impact) is expected from the coating solution F11 compared to F12; spray coating is expected to be a better option when coating the activated mesh with F11. Despite the significant differences in the apparent surface roughness features in Figure 7(c) and (d), the difference in the WCA for these two mesh samples

is not statistically significant at a 95% confidence level; however, the roughness shown in Figure 7(d) can facilitate the separation of disperse oil-in-water droplets.

In Figure 8, we demonstrate approximate size analysis of the flower-like surface roughness for a given part of the mesh sample with eight mesh openings, coated with F12 solution. For comparison, we also show the 200 μm scale bar. This SEM picture is obtained at the 500X magnification level. We fit a circle to the mesh pore opening without considering the coating, which is shown with dashed yellow circles (see Figure 8). For each mesh opening, another circle is also indicated with solid white color that is fitted to the available pore opening at the condition corresponding to the breakthrough of the non-wetting phase. Figure 8 depicts (approximate) uncoated mesh opening diameter of 75.4 μm – 77.7 μm with an average of (76.4±0.6) μm that is reduced to 45.5 μm – 50.5 μm for the coated mesh, with an average diameter of (48.3±1.7) μm.

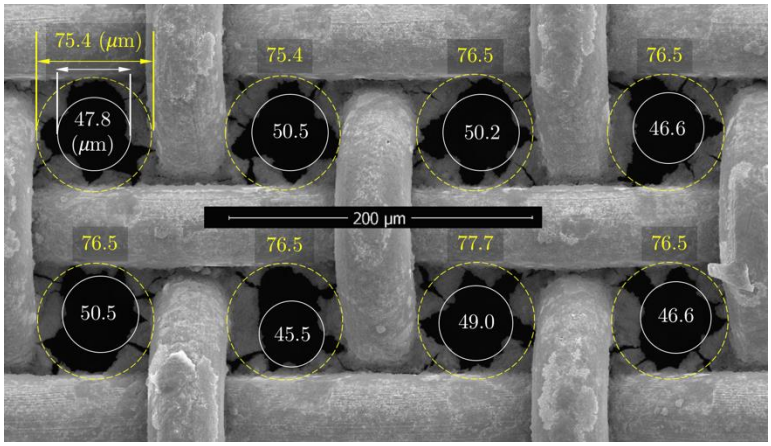

Figure 8. A schematic of the flower-like roughness features of the SHSO mesh (coated with F12). The dashed yellow circles are approximately fitted to the mesh opening, and the white circles are fitted to the pore opening, corresponding to the breakthrough condition for the non-wetting phase. The numbers in the figure show diameter in μm.

X-ray diffraction (XRD): Figure 9 shows an overlay of the XRD patterns for three cases, including cleaned mesh, silanized mesh (coating solution F7), and coated mesh (coating solution F12). The main

diffraction peaks are located at 43.4˚, 44.7˚, 50.9˚, and 74.7˚ which can be attributed to γ (111), α (110), γ (200), and γ (220), respectively; furthermore, there are two minor peaks at 64.9˚and 82.4˚that can be attributed to α (200) and α (211) [58]. The locations of the diffraction peaks are in agreement with those obtained in XRD spectrum of AISI 316 grade SS plate from Qin et al. [58]. As it is clear in Figure 9, the silane solution F7 and the coating solution F12 do not shift the position of diffraction peaks, while there are some minor effects on the intensity of peaks. It means that both coating solutions (F7 and F12) neither diffract the X-ray nor affect the crystalline structure of the AISI 316 SS. These similarities between the peaks of AISI 316 SS (bare mesh) and coated mesh (F12) confirm the amorphous structure of the mesh coating, including the solid particles that are used to alter the surface roughness. Hence, this observation also confirms that the silica nanoparticles (Aerosil® R812), utilized in coating solution F12, are amorphous; they do not affect the crystallinity of the bare mesh.

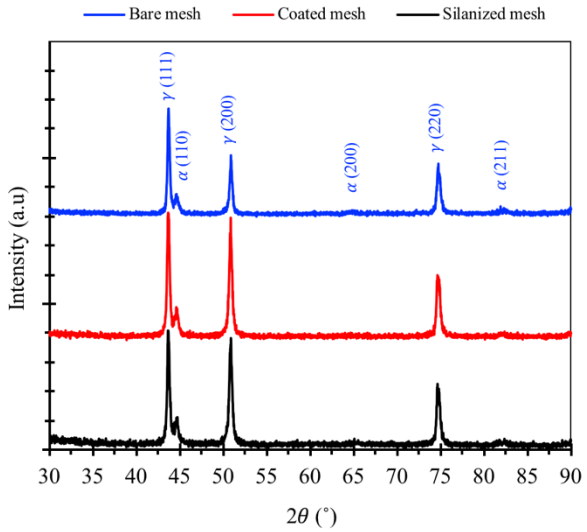

Figure 9. Overlay of XRD patterns for the clean mesh (blue), silanized mesh (red), and mesh coated with F12 (black); γ and α are atheneite and martensite steel phases, respectively.

Energy-dispersive X-ray spectroscopy (EDX): In Figure 10, we show the EDX analysis of the mesh coated with F12 formulation. The weight percent of the elements and standard deviation (σ) are also

reported in Figure 10; the highest detected element counts and X-ray energy belongs to Si with 56.11 wt% of the detected sample area at an energy level of 1.74 keV. For the EDX analysis, we choose an area-of-interest on the coated mesh wires and dismiss the mesh empty area that has no coating. The wt% of Si in the long-chain silane is less than 3 wt%. The NPs are fumed silica (SiO_2) for which their surface area is functionalized with hexamethyldisilazane (HMDS). The ratio of Si/F in the coating is much higher than that in the silane, confirming that the NPs are successfully bonded onto the mesh surface.

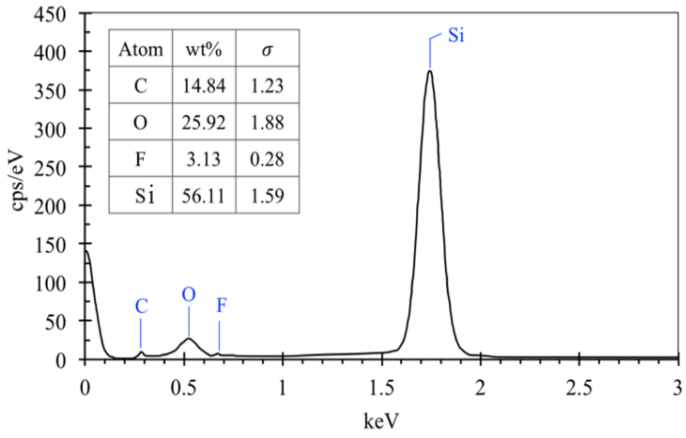

Figure 10. EDX analysis of the SHSO mesh coating (F12).

Fourier-transform infrared spectroscopy (FTIR): The FTIR transmittance for the SHSO mesh coated with F12 solution is demonstrated in Figure 11 in the wavelength range 400 cm^{-1} to 4000 cm^{-1}. A large band with a strong peak is observed at 452 cm^{-1}, which is due to Si-O-Si rocking [59]. The absorption band at 807 cm^{-1} corresponds to the Si-O-Si bending; the O-Si-O bending gives an IR peak at about 475 cm^{-1} [60]. The strong absorption at 1060 cm^{-1} is due to the stretching of the Si-O-Si bond [61]. These three intense absorption peaks at 452, 807, and 1060 cm^{-1} are due to the silica NPs on the coated mesh surface. The peak around 700 cm^{-1} is due to the vibration of the $–CH_2$ groups for the silane-modified silica NPs, and the absorption peak at 895 corresponds to the deformation of Si-OH bonds [62]. Furthermore, the peaks at 1240 cm^{-1} and 1150 cm^{-1} are attributed to the C-F asymmetric stretching

vibrations for the -CF_2- and –CF_3 groups, respectively [63]. The peak at 1190 cm^{-1} may be assigned to the symmetrical stretching of the CF-F bonds [64]. The absorption peak for the stretching of bond Si-CH_3 (in NPs) is not observed at ~1297 cm^{-1} (detected in the FTIR spectra of the NPs) [61], implying that the NPs are completely hydrolyzed in the final coating. The broad (but weak) absorption band in the range 2890–3680 cm^{-1} is a characteristic of the O-H stretching from water vapor [65]; the weak band around 1482 cm^{-1} is also attributed to the adsorbed water [62].

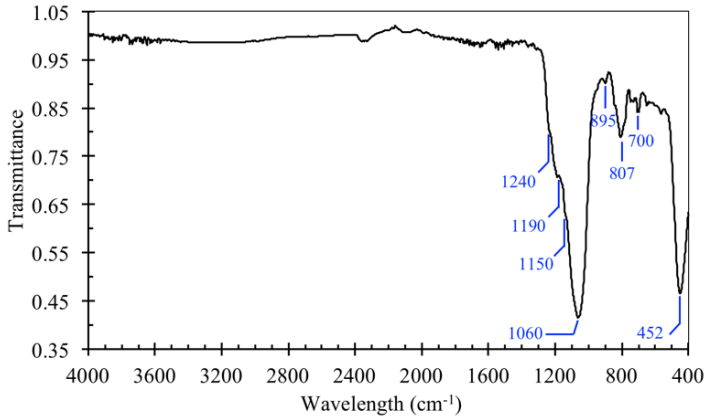

Figure 11. FTIR spectra of the SHSO mesh (coated with F12) in wavelength range 400 to 4000 cm^{-1}.

4.3 Mesh chemical stability analysis

The stability of the SHSO mesh against chemicals can be assessed by WCA measurements, after aging the coated mesh in harsh environments. The static contact angle results for the SS mesh coated with the solution F12 are provided in Figure 12 for which the samples are aged over a 4-week period in 0.1 M acid (H_2SO_4), 0.1 M alkaline (NaOH), and 1 M brine (NaCl) solutions. The contact angle measurements reported in Figure 12 are the average of five replicates (mesh samples); onto each mesh sample, we dispense three drops. Prior to aging in acid, alkaline, and brine solutions, the WCA=163.8˚±1.8˚. After one week, the WCA is not significantly affected for the sample aged in 1 M NaCl solution; however, the WCA is dropped to 153.9˚±1.8˚ for 0.1 M H_2SO_4-aged mesh and to 154.4˚±0.8˚ for 0.1 M NaOH-aged mesh sample. There is not a remarkable change in the surface wettability upon exposure to the acid, after

this early effect on the coating. For instance, the WCA after four weeks is marginally reduced to 151.6˚±1.2˚, considering the variability in the measurements. The WCA for the mesh samples aged in the brine slightly decreases over time (e.g., the contact angle for the brine-aged mesh is 159.2˚±0.8˚ after four weeks). The effect of alkaline solution on the mesh coating is the most significant such that WCA=145.9˚±1.7˚ after four weeks of aging. In agreement with the literature [66], the hydrophobicity of the silica-based surfaces declines in strong alkaline solutions due to its effect on the Si-O-Si bonding.

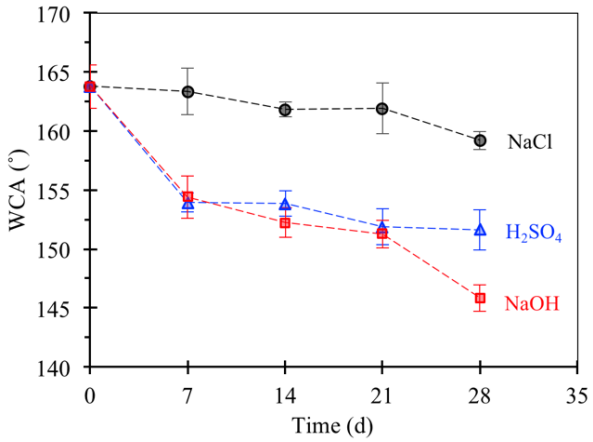

Figure 12. Chemical stability analysis through WCA measurements. The SHSO mesh samples are aged at room temperature in H_2SO_4 (0.1 M, shown in blue), NaOH (0.1 M, shown in red), and brine (1 M, shown in black) solutions over four weeks. The markers indicate the average of contact angle values for five replicates.

We also examine the chemical stability analysis in extremely concentrated acid and alkaline solutions where the concentration is 1 M. Similar to the chemical stability tests using 0.1 M chemicals, five replication samples of the mesh are considered where three water droplets are placed on each mesh (on different locations). A significant effect by 1 M NaOH solution on the mesh coating is observed; after one week, the WCA drops to 93.4˚±6.2˚. Not only the contact angle is considerably altered by the 1 M alkaline solution, the variability in the WCA measurements is also drastically increased. If the water-mesh contact is influenced by concentrated NaOH solution, a loss of hydrophobicity is observed, resulting in WCA reduction. We observe a high standard deviation of S=10.9˚ for the mesh samples aged

for one week in 1 M NaOH solution, which is significantly higher than $S<1^{\circ}$ attained for the samples aged in 0.1 M NaOH solution (after one week). When the mesh samples are placed in 1 M H_2SO_4 solution, the strong acid does not affect the mesh coating; after 1-week aging, WCA=152.5˚±1.0˚ is observed. The standard deviation for the mesh samples aged in 1 M acid solution is one order of magnitude lower. Therefore, the mesh coating is not significantly influenced by highly concentrated acid.

The difference in the chemical stability of the SHSO mesh against 1 M acid and 1 M alkaline solutions is also confirmed by the SEM pictures, as depicted in Figure 13.

(a) H_2SO_4 (1.0 M) (b) NaOH (1.0 M)

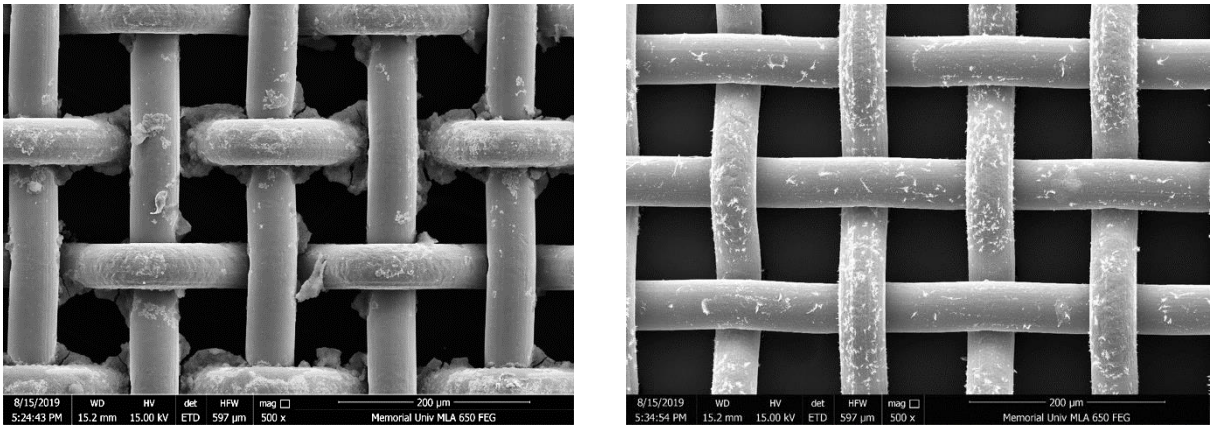

Figure 13. Scanning electron microscopy pictures (at 500X magnification) of the SHSO mesh exposed to: (a) 1.0 M H_2SO_4, and (b) 1.0 M NaOH for one week.

The SEM images shown in Figure 13 are obtained at 500X magnification, and the scale bar is 200 μm. There are some differences between the flower-like roughness features (compared to those in Figure 7(d)), due to handling and reaction with the concentrated acid solution. Although the change in surface roughness affects the capillary pressure for the retention of the wetting phase (oil), it does not considerably alter the contact angle. On the contrary, the mesh sample aged in 1 M NaOH solution

experiences significant dissolution of the coating in strong alkaline solution (see Figure 13(b)), which is in agreement with the WCA measurements.

Strong alkaline solutions (pH>13) with active OH^- ions can have detrimental effects on silica aggregates with poor crystallinity [67]. For our coating, such a potential is possible for the micro-nanoparticle aggregates of amorphous silica. Also, the OH^- ions in strong alkaline solution can attack the Si-O-Si bonds that connect adjacent silane groups, weakening the 3D network of silane functional groups. Moreover, the OH^- ions can remove the fluorinated functional groups from the mesh surface by breaking the Si-O bonds that are attached to the mesh surface (see Figure 2), causing partial de-hydrolysis [67]. Therefore, the coated mesh loses its superhydrophobicity strength due to possible reactions between the silicon and a strong alkali.

4.4 Oil-water separation test

The oil-water separation is conducted according to the process flow diagram shown in Figure 3(a). The actual picture of the set-up is given in Figure 3(b). Kerosene is used to simulate a free oil in water mixture that permeates through the fabricated SHSO mesh tube. The oil phase remains as a free phase over the water surface. The water phase is expected to be blocked from permeating through the SHSO membrane at pressures lower than the breakthrough capillary pressure of the water phase. As soon as the water wets the mesh tube, it starts draining out of the glass tube through the mesh. The oil is collected in the beaker with an excellent separation efficiency > 99%, whereas the water is blocked around the tube mesh. The permeation of the water into the mesh under gravity drainage is not observed. Capillary pressure contrast between the oil-air and water-air phases is one of the important mechanisms (and driving forces) in governing the efficiency of oil-water separation process through SHSO membranes. The capillary pressure between the wetting and non-wetting phases is calculated using the Young-Laplace equation:

$$\Delta P = -4\gamma cos\theta/d \quad (1)$$

where ΔP (N/m^2) is the intrusion pressure, the excess pressure required for the water/oil phase to wet the SHSO mesh tube; γ resembles the interfacial tension (N/m) of fluid pairs; θ is the WCA of the SHSO mesh; and d represents the pore size diameter (m). The positive intrusion pressure (θ > 90°) indicates that the water as the non-wetting phase requires an extra pressure to pass through the mesh pores, conversely the oil phase as the wetting phase with a negative intrusion pressure (θ < 90°) requires no extra pressure to wet the SHSO mesh tube [68]. In the separation tests, we repeat the experiments with kerosene four times, and the separation efficiency is (99.0±0.6) % in a period of 1 min. In a follow-up study, we can systematically investigate the dynamics of oil-water separation in the same mesh shown in Figure 3(b), where the effects of flow rate, oil-to-water ratio, and oil dispersion are assessed. We also use the effect of vacuum on the permeate phase to accelerate the oil permeation. For the case of kerosene, the gravity-based separation is fast; however, for more viscose oils (crude oil or vegetable oil), the oil permeation rate through the membrane will dictate the size of the separation unit.

5 CONCLUSIONS

We fabricate a superhydrophobic-superoleophilic (SHSO) stainless steel mesh-based membrane through a facile dip-coating technique, and use the membrane for oil-water separation application. The effect of silane alkyl-chain length by using a short-chain silane (Dynasylan® Sivo 408), and a long-chain silane (Dynasylan® F8261) on the water contact angle (WCA) is studied. We also investigate the influence of solid composition in the coating (1 wt% solid in liquid coating solution) with hydrophobic nanoparticles (NPs, Aerosil® R812) and microparticles (MPs, SIPERNAT® D13) on the wetness characteristic of the mesh. A total number of 12 coating formulations are tested by varying the silane and solid compositions. The following conclusions are drawn based on the research outputs:

- The WCA results show that at all solid compositions, the long silane generates a more hydrophobic surface than the short silane.
- A maximum in the WCA is observed with both silanes for a solid mixture, containing 75 wt% NPs and 25 wt% MPs. The maximum WCA for the long silane is 165.8˚±2.0˚, which is not statistically different from that for the short silane. By increasing the contribution of the NPs to 100%, the WCA decreases for both silanes; however, this reduction is more significant for the short silane. Therefore, it is possible to achieve a similar hydrophobicity with a shorter silane that contains less F atoms (less harmful) by adjusting the composition of the solid part of the coating.
- According to the SEM images, the flower-like hierarchical micro- and nano-roughness with a high capillary pressure for the coating solution that contains only NPs (1 wt% in the coating) is attained.
- The 4-week stability tests exhibit an excellent chemical resistance of the SHSO mesh to H_2SO_4 (0.1 and 1 M), NaCl (1 M), and NaOH (0.1 M), where WCA>145˚ after four weeks. The alkaline solution affects the coating more; the majority of the changes to the hydrophobicity occurs during the first week in all cases. However, loss of hydrophobicity is observed after 1-week exposure to 1 M NaOH.
- The as-fabricated SHSO mesh separates kerosene from an oil-water mixture with an efficiency of greater than 99%.
- The proposed fabrication of the SHSO mesh is simple, facile, low-cost, and effective that has applications in selective oil-water separation.

The recommendations for the future research investigation are: 1) it might be a good recommendation to conduct surface modification tests using non-chemical techniques, such as laser or 3D printers, and then compare the magnitudes of contact angles attained from different approaches; 2) continuous and dynamic oil-water separation tests using SHSO mesh tubes are suggested to meet the demand in treating industrial oily wastewater. The effects of flow rate, oil concentration, oil dispersion, and surfactant in the mixture can be also studied; 3) we suggest a follow-up study to scale up the oil-water separator through a horizontal shell-and-tube configuration. The allocation of the permeate (oil) phase to either shell or tube side is a design decision that appears to be interesting; 4) applying a vacuum to the permeate phase can accelerate the continuous oil-water separation; and 5) the study of water-based solid contaminations and fouling performance of the SHSO mesh is of high interest for several researchers in the field of water and wastewater treatment. It is expected that the fine solid particles suspended in the water phase to be retained in the aqueous phase away from the surface of the mesh tube, since water cannot wet the surface of the coated mesh.

ACKNOWLEDGEMENTS

The financial assistance from the Natural Sciences and Engineering Research Council of Canada (NSERC), InnovateNL, Equinor Canada, Terra Nova Young Innovator Award, and Memorial University are appreciated. The authors thank Evonik Industries AG for providing fumed silica and silane samples. We also acknowledge the help from Dr. Yahui Zhang and Mr. Rene Silva for conducting FTIR tests.

NOMENCLATURES

Acronyms

DI	Deionized

DMS	Dimethyl siloxane
EDX	Energy-dispersive X-ray spectroscopy
FTIR	Fourier-transform infrared spectroscopy
ID	Inner diameter
MPs	Microparticles
NPs	Nanoparticles
OD	Outer diameter
PDA	Polydopamine
PDMS	Polydimethylsiloxane
PFAS	Perfluoroalkylsilane
PFTOS	Perfluorooctyltriethoxysilane
PTFE	Polytetrafluoroethylene
SEM	Scanning electron microscope
SHSO	Superhydrophobic and superoleophilic
SS	Stainless steel
WCA	Water contact angle
XRD	X-ray diffraction

Variables/Symbols

d	Pore size diameter	m
P	Pressure	N/m^2 or Pa

Greek Letters

ΔP	Pressure difference	N/m^2 or Pa
γ	Oil/water interfacial tension	N/m
θ	Contact angle	(°)

REFERENCES

[1] Wang Q, Cui Z, Xiao Y, Chen Q. Stable highly hydrophobic and oleophilic meshes for oil–water separation2007.

[2] Du Z, Ding P, Tai X, Pan Z, Yang H. Facile Preparation of Ag-Coated Superhydrophobic/Superoleophilic Mesh for Efficient Oil/Water Separation with Excellent Corrosion Resistance. Langmuir. 2018;34:6922-9.

[3] Varshney P, Nanda D, Satapathy M, Mohapatra SS, Kumar A. A facile modification of steel mesh for oil–water separation. New Journal of Chemistry. 2017;41:7463-71.

[4] Feng L, Zhang Z, Mai Z, Ma Y, Liu B, Jiang L, et al. A super-hydrophobic and super-oleophilic coating mesh film for the separation of oil and water. Angewandte Chemie (International ed in English). 2004;43:2012-4.

[5] Li H, Zheng M, Ma L, Zhu C, Lu S. Two-dimensional ZnO nanoflakes coated mesh for the separation of water and oil. Materials Research Bulletin. 2013;48:25-9.

[6] Liu Y, Zhang K, Yao W, Liu J, Han Z, Ren L. Bioinspired structured superhydrophobic and superoleophilic stainless steel mesh for efficient oil-water separation. Colloids and Surfaces A: Physicochemical and Engineering Aspects. 2016;500:54-63.

[7] Xiang M, Jiang M, Zhang Y, Liu Y, Shen F, Yang G, et al. Fabrication of a novel superhydrophobic and superoleophilic surface by one-step electrodeposition method for continuous oil/water separation. Applied Surface Science. 2018;434:1015-20.

[8] Matin A, Baig U, Gondal MA, Akhtar S, Zubair SM. Superhydrophobic and superoleophilic surfaces prepared by spray-coating of facile synthesized Cerium(IV) oxide nanoparticles for efficient oil/water separation. Applied Surface Science. 2018;462:95-104.

[9] Cao W-T, Liu Y-J, Ma M-G, Zhu J-F. Facile preparation of robust and superhydrophobic materials for self-cleaning and oil/water separation. Colloids and Surfaces A: Physicochemical and Engineering Aspects. 2017;529:18-25.

[10] Matin A, Baig U, Gondal MA, Akhtar S, Zubair SM. Facile fabrication of superhydrophobic/superoleophilic microporous membranes by spray-coating ytterbium oxide particles for efficient oil-water separation. Journal of Membrane Science. 2018;548:390-7.

[11] Yang H, Zhang X, Cai Z-Q, Pi P, Zheng D, Wen X, et al. Functional silica film on stainless steel mesh with tunable wettability. Surface and Coatings Technology. 2011;205:5387-93.

[12] Zhang Y, Wang X, Wang C, Liu J, Zhai H, Liu B, et al. Facile fabrication of zinc oxide coated superhydrophobic and superoleophilic meshes for efficient oil/water separation. RSC Advances. 2018;8:35150-6.

[13] Yang J, Tang Y, Xu J, Chen B, Tang H, Li C. Durable superhydrophobic/superoleophilic epoxy/attapulgite nanocomposite coatings for oil/water separation. Surface and Coatings Technology. 2015;272:285-90.

[14] Qin F, Yu Z, Fang X, Liu X, Sun X. A novel composite coating mesh film for oil-water separation. Frontiers of Chemical Engineering in China. 2009;3:112-8.

[15] Wang C-F, Tzeng F-S, Chen H-G, Chang C-J. Ultraviolet-Durable Superhydrophobic Zinc Oxide-Coated Mesh Films for Surface and Underwater–Oil Capture and Transportation. Langmuir. 2012;28:10015-9.

[16] Xiao C, Si L, Liu Y, Guan G, Wu D, Wang Z, et al. Ultrastable coaxial cable-like superhydrophobic mesh with self-adaption effect: facile synthesis and oil/water separation application. Journal of Materials Chemistry A. 2016;4:8080-90.

[17] Wu J, Chen J, Qasim K, Xia J, Lei W, Wang B-p. A hierarchical mesh film with superhydrophobic and superoleophilic properties for oil and water separation. Journal of Chemical Technology & Biotechnology. 2012;87:427-30.

[18] Lee C, Baik S. Vertically-aligned carbon nano-tube membrane filters with superhydrophobicity and superoleophilicity. Carbon. 2010;48:2192-7.

[19] Lee CH, Johnson N, Drelich J, Yap YK. The performance of superhydrophobic and superoleophilic carbon nanotube meshes in water–oil filtration. Carbon. 2011;49:669-76.

[20] Crick CR, Gibbins JA, Parkin IP. Superhydrophobic polymer-coated copper-mesh; membranes for highly efficient oil–water separation. Journal of Materials Chemistry A. 2013;1:5943-8.

[21] Feng L, Zhang Z, Mai Z, Ma Y, Liu B, Jiang L, et al. A Super-Hydrophobic and Super-Oleophilic Coating Mesh Film for the Separation of Oil and Water. Angewandte Chemie. 2004;116:2046-8.

[22] Ju J, Wang T, Wang Q. A facile approach in fabricating superhydrophobic and superoleophilic poly (vinylidene fluoride) membranes for efficient water–oil separation. Journal of Applied Polymer Science. 2015;132.

[23] La D-D, Nguyen TA, Lee S, Kim JW, Kim YS. A stable superhydrophobic and superoleophilic Cu mesh based on copper hydroxide nanoneedle arrays. Applied Surface Science. 2011;257:5705-10.

[24] Pi P, Hou K, Zhou C, Li G, Wen X, Xu S, et al. Superhydrophobic Cu2S@Cu2O film on copper surface fabricated by a facile chemical bath deposition method and its application in oil-water separation. Applied Surface Science. 2017;396:566-73.

[25] Yu L, Zhang S, Zhang M, Chen J. Superhydrophobicity construction with dye-sensitised TiO2 on fabric surface for both oil/water separation and water bulk contaminants purification. Applied Surface Science. 2017;425:46-55.

[26] Xue C-H, Ji P-T, Zhang P, Li Y-R, Jia S-T. Fabrication of superhydrophobic and superoleophilic textiles for oil–water separation. Applied Surface Science. 2013;284:464-71.

[27] Zhang X, Geng T, Guo Y, Zhang Z, Zhang P. Facile fabrication of stable superhydrophobic SiO2/polystyrene coating and separation of liquids with different surface tension. Chemical Engineering Journal. 2013;231:414-9.

[28] Liu H, Huang J, Chen Z, Chen G, Zhang K-Q, Al-Deyab SS, et al. Robust translucent superhydrophobic PDMS/PMMA film by facile one-step spray for self-cleaning and efficient emulsion separation. Chemical Engineering Journal. 2017;330:26-35.

[29] Chakradhar RPS, Kumar VD, Rao JL, Basu BJ. Fabrication of superhydrophobic surfaces based on ZnO–PDMS nanocomposite coatings and study of its wetting behaviour. Applied Surface Science. 2011;257:8569-75.

[30] Zhang M, Wang C, Wang S, Li J. Fabrication of superhydrophobic cotton textiles for water–oil separation based on drop-coating route. Carbohydrate polymers. 2013;97:59-64.

[31] Cao M, Luo X, Ren H, Feng J. Hot water-repellent and mechanically durable superhydrophobic mesh for oil/water separation. Journal of Colloid and Interface Science. 2018;512:567-74.

[32] Wang S, Li M, Lu Q. Filter Paper with Selective Absorption and Separation of Liquids that Differ in Surface Tension. ACS Applied Materials & Interfaces. 2010;2:677-83.

[33] Qing W, Shi X, Deng Y, Zhang W, Wang J, Tang CY. Robust superhydrophobic-superoleophilic polytetrafluoroethylene nanofibrous membrane for oil/water separation. Journal of Membrane Science. 2017;540:354-61.

[34] Shang Y, Si Y, Raza A, Yang L, Mao X, Ding B, et al. An in situ polymerization approach for the synthesis of superhydrophobic and superoleophilic nanofibrous membranes for oil–water separation. Nanoscale. 2012;4:7847-54.

[35] Zhang W, Lu X, Xin Z, Zhou C. A self-cleaning polybenzoxazine/TiO2 surface with superhydrophobicity and superoleophilicity for oil/water separation. Nanoscale. 2015;7:19476-83.

[36] Yu T, Lu S, Xu W, Boukherroub R. Preparation of superhydrophobic/superoleophilic copper coated titanium mesh with excellent ice-phobic and water-oil separation performance. Applied Surface Science. 2019;476:353-62.

[37] Wei C, Dai F, Lin L, An Z, He Y, Chen X, et al. Simplified and robust adhesive-free superhydrophobic SiO2-decorated PVDF membranes for efficient oil/water separation. Journal of Membrane Science. 2018;555:220-8.

[38] Mi H-Y, Jing X, Xie H, Huang H-X, Turng L-S. Magnetically driven superhydrophobic silica sponge decorated with hierarchical cobalt nanoparticles for selective oil absorption and oil/water separation. Chemical Engineering Journal. 2018;337:541-51.

[39] Hou W, Mu B, Wang Q. Studies on wettability of polypropylene/methyl-silicone composite film and polypropylene monolithic material. Journal of Colloid and Interface Science. 2008;327:120-4.

[40] Darmanin T, Nicolas M, Guittard F. Electrodeposited polymer films with both superhydrophobicity and superoleophilicity. Physical Chemistry Chemical Physics. 2008;10:4322-6.

[41] Hsieh C-T, Hsu J-P, Hsu H-H, Lin W-H, Juang R-S. Hierarchical oil–water separation membrane using carbon fabrics decorated with carbon nanotubes2016.

[42] Shi Z, Zhang W, Zhang F, Liu X, Wang D, Jin J, et al. Ultrafast Separation of Emulsified Oil/Water Mixtures by Ultrathin Free-Standing Single-Walled Carbon Nanotube Network Films. Advanced Materials. 2013;25:2422-7.

[43] Kaur H, Bulasara VK, Gupta RK. Influence of pH and temperature of dip-coating solution on the properties of cellulose acetate-ceramic composite membrane for ultrafiltration. Carbohydrate Polymers. 2018;195:613-21.

[44] Nandi BK, Uppaluri R, Purkait MK. Effects of dip coating parameters on the morphology and transport properties of cellulose acetate–ceramic composite membranes. Journal of Membrane Science. 2009;330:246-58.

[45] Wang Q, Cui Z, Xiao Y, Chen Q. Stable highly hydrophobic and oleophilic meshes for oil–water separation. Applied Surface Science. 2007;253:9054-60.

[46] Zhang L, Chen H, Sun J, Shen J. Layer-by-Layer Deposition of Poly(diallyldimethylammonium chloride) and Sodium Silicate Multilayers on Silica-Sphere-Coated Substrate—Facile Method to Prepare a Superhydrophobic Surface. Chemistry of Materials. 2007;19:948-53.

[47] Zhang H, Zeng X, Gao Y, Shi F, Zhang P, Chen J-F. A facile method to prepare superhydrophobic coatings by calcium carbonate. Industrial & engineering chemistry research. 2011;50:3089-94.

[48] Barati Darband G, Aliofkhazraei M, Khorsand S, Sokhanvar S, Kaboli A. Science and Engineering of Superhydrophobic Surfaces: Review of Corrosion Resistance, Chemical and Mechanical Stability. Arabian Journal of Chemistry. 2018.

[49] Sun ZD, Yang YN, Li QK, Liu JG, Xu Q, Yan CW. Optimization of mixed silanes agent solution and curing process for composite γ-glycidoxypropyl trimethoxysilane (γ-GPS)/bis-1.2-(triethoxysilyl)ethane (BTSE) silane film on Q235 steel surface. Materialwissenschaft und Werkstofftechnik. 2020;51:480-7.

[50] Ng WF, Wong MH, Cheng FT. Stearic acid coating on magnesium for enhancing corrosion resistance in Hanks' solution. Surface and Coatings Technology. 2010;204:1823-30.

[51] Wang C, Yao T, Wu J, Ma C, Fan Z, Wang Z, et al. Facile approach in fabricating superhydrophobic and superoleophilic surface for water and oil mixture separation. ACS applied materials & interfaces. 2009;1:2613-7.

[52] Pan Q, Wang M, Wang H. Separating small amount of water and hydrophobic solvents by novel superhydrophobic copper meshes. Applied Surface Science. 2008;254:6002-6.

[53] Fan H, Wright A, Gabaldon J, Rodriguez A, Brinker CJ, Jiang YB. Three-Dimensionally Ordered Gold Nanocrystal/Silica Superlattice Thin Films Synthesized via Sol–Gel Self-Assembly. Advanced Functional Materials. 2006;16:891-5.

[54] Mostefaï M, Auriac Y, Shanahan M, Bressan J, Meslif A. Fluoroalkylsilanes as non-stick coatings: adhesion of glucose and its thermal byproducts. International journal of adhesion and adhesives. 1998;18:273-81.

[55] Sarbada S, Shin YC. Superhydrophobic contoured surfaces created on metal and polymer using a femtosecond laser. Applied Surface Science. 2017;405:465-75.

[56] Ha C-S, Nagappan S. Hydrophobic and Superhydrophobic Organic-Inorganic Nano-Hybrids: Pan Stanford; 2018.

[57] Gao T, Meng G, Wang Y, Sun S, Zhang L. Electrochemical synthesis of copper nanowires. Journal of Physics: Condensed Matter. 2001;14:355-63.

[58] Qin W, Li J, Liu Y, Yue W, Wang C, Mao Q, et al. Effect of rolling strain on the mechanical and tribological properties of 316 L stainless steel. Journal of Tribology. 2019;141.

[59] Brito JB, Costa TMH, Rodembusch FS, Balzaretti NM. Photoluminescence of silica monoliths prepared from cold sintering of nanometric aerosil precursors under high pressure. Journal of Luminescence. 2017;187:154-9.

[60] Wood D, Rabinovich EM. Study of alkoxide silica gels by infrared spectroscopy. Applied Spectroscopy. 1989;43:263-7.

[61] Sanaeepur H, Kargari A, Nasernejad B. Aminosilane-functionalization of a nanoporous Y-type zeolite for application in a cellulose acetate based mixed matrix membrane for CO2 separation. RSC Advances. 2014;4:63966-76.

[62] Ambrożewicz D, Ciesielczyk F, Nowacka M, Karasiewicz J, Piasecki A, Maciejewski H, et al. Fluoroalkylsilane versus alkylsilane as hydrophobic agents for silica and silicates. Journal of Nanomaterials. 2013;2013.

[63] Lu Y, Sathasivam S, Song J, Chen F, Xu W, Carmalt CJ, et al. Creating superhydrophobic mild steel surfaces for water proofing and oil–water separation. Journal of Materials Chemistry A. 2014;2:11628-34.

[64] Rajab FH, Liauw CM, Benson PS, Li L, Whitehead KA. Production of hybrid macro/micro/nano surface structures on Ti6Al4V surfaces by picosecond laser surface texturing and their antifouling characteristics. Colloids and Surfaces B: Biointerfaces. 2017;160:688-96.

[65] Limcharoen A, Limsuwan P, Pakpum C, Siangchaew K. Characterisation of Câ□“F Polymer Film Formation on the Air-Bearing Surface Etched Sidewall of Fluorine-Based Plasma Interacting with ALOâ□“TiC Substrate. Journal of Nanomaterials. 2013;2013.

[66] Das I, De G. Zirconia based superhydrophobic coatings on cotton fabrics exhibiting excellent durability for versatile use. Scientific Reports. 2015;5:18503.

[67] Murray CD. Durability of silane sealer in a highly alkaline environment. 2014.

[68] Cai Y, Li S, Cheng Z, Xu G, Quan X, Zhou Y. Facile fabrication of super-hydrophobic FAS modified electroless Ni-P coating meshes for rapid water-oil separation. Colloids and Surfaces A: Physicochemical and Engineering Aspects. 2018;540:224-32.